Inorganic Chemistry

Article

pubs.acs.org/IC

Bifunctional Mixed-Lanthanide Cyano-Bridged Coordination Polymers $Ln_{0.5}Ln'_{0.5}(H_2O)_5[W(CN)_8]$ (Ln/Ln′ = Eu^{3+}/Tb^{3+}, Eu^{3+}/Gd^{3+}, Tb^{3+}/Sm^{3+})

Elena Chelebaeva,[†,∥] Jérôme Long,[†] Joulia Larionova,*[,†] Rute A. S. Ferreira,[‡] Luis D. Carlos,*[,‡] Filipe A. Almeida Paz,[§] José B. R. Gomes,[§] Alexander Trifonov,[∥] Christian Guérin,[†] and Yannick Guari[†]

[†]Institut Charles Gerhardt Montpellier, UMR 5253 CNRS-UM2-ENSCM-UM1, Chimie Moléculaire et Organisation du Solide, Université Montpellier II, Place E. Bataillon, 34095 Montpellier cedex 5, France

[‡]Departamento de Física and CICECO, Universidade de Aveiro, 3810 -193 Aveiro, Portugal

[§]Departamento de Química and CICECO, Universidade de Aveiro, 3810 -193 Aveiro, Portugal

[∥]G. A. Razuvaev Institute of Organometallic Chemistry of the Russian Academy of Science, Tropinina 49, GSP-44S, 603950, Nizhny Novgorod, Russia

Supporting Information

ABSTRACT: A new family of mixed-lanthanide cyano-bridged coordination polymers $Ln_{0.5}Ln'_{0.5}(H_2O)_5[W(CN)_8]$ (where Ln/Ln′ = Eu^{3+}/Tb^{3+}, Eu^{3+}/Gd^{3+}, and Tb^{3+}/Sm^{3+}) containing two lanthanide and one transition metal ions were obtained and characterized by X-ray diffraction, photoluminescence spectroscopy, magnetic analyses, and theoretical computation. These compounds are isotypical and crystallize in the tetragonal system *P4/nmm* forming two-dimensional grid-like networks. They present a magnetic ordering at low temperature and display the red Eu^{3+} ($^5D_0 \rightarrow {}^7F_{0-4}$) and green Tb^{3+} ($^5D_4 \rightarrow {}^7F_{6-2}$) characteristic photoluminescence. The $Tb_{0.5}Eu_{0.5}(H_2O)_5[W(CN)_8]$ compound presents therefore green and red emission and shows Tb^{3+}-to-Eu^{3+} energy transfer.

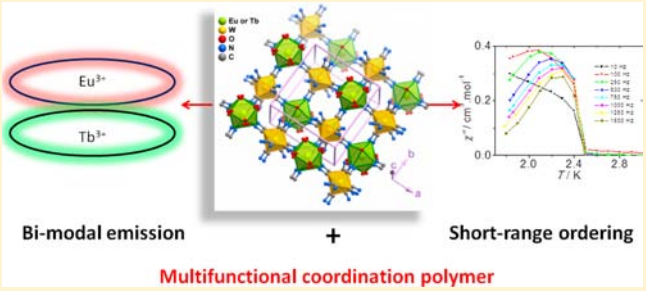

1. INTRODUCTION

Multifunctional materials combining a few useful physical or chemical properties in the same structure able to demonstrate different physical responses to external stimuli have attracted a great deal of attention in recent years due to their fundamental interest and their potential applications.[1] Among these, molecule-based materials designed by self-assembly reactions from functional building blocks are excellent candidates to create and explore multifunctionality. Advances for such materials were made by numerous associations such as the magnetic order with optical activity,[2] nonlinear optical activity[3] and conductivity[4] or porosity with luminescence,[5] electronic switching,[6] magnetic ordering,[7] and conductivity,[8] among others. However, molecule-based materials combining magnetic ordering and luminescence are rare, and a relatively small number of reports on host−guest hybrid compounds in which luminescent organic chromophores or photoactive complexes such as $[Ru(bipy)_3]^{3+}$ (bipy = 2,2′ bipyridil) are intercalated between magnetic layers assembled from transition metal ions can be cited.[9]

Recently, we started to investigate a new family of magneto-luminescent coordination polymers based on luminescent lanthanide ions and paramagnetic octacyanomalybdate(V) or octacyanotungstate(V) building blocks.[10] Several points justify such association. First, the paramagnetic lanthanides have a large unquenched orbital moment associated with internal *f* magnetic orbitals giving rise to high magnetic anisotropy which is interesting for the design of magnetically ordered networks with high coercivity.[11] On the other hand, due to the "core character" of the 4*f* orbitals, magnetic interactions involving lanthanide ions are relatively weak, and an association thereof with paramagnetic molybdenum or tungsten ions should increase the strength of magnetic interactions in one hand and reduce the problem of orbital degeneracy on the other. Second, *f-f* transitions of Ln^{3+} ions are spin and parity forbidden,[12] and in order to prevent the quenching of the Ln^{3+} luminescence by energy transfer processes, octacyanomolybdate or tungstate building blocks are suitable because they do not absorb efficiently Ln^{3+} visible emitted light, not acting therefore as dense filters. Consequently, a new family of two-dimensional compounds having the general formula $Ln(H_2O)_5[M(CN)_8]$ (Ln = Tb^{3+}, Eu^{3+}, Sm^{3+}, Gd^{3+}; M = Mo^{5+}, W^{5+}) was investigated.[10a,b] These compounds present long-range magnetic ordering at low temperature, except the Eu^{3+}-containing compounds. Tb^{3+}- and Eu^{3+}-containing coordination polymers show characteristic luminescence ($^5D_4 \rightarrow {}^7F_{6-2}$ and $^5D_0 \rightarrow {}^7F_{0-4}$ transitions, for Tb^{3+} and Eu^{3+}, respectively) in

Received: May 31, 2012
Published: August 1, 2012

   dx.doi.org/10.1021/ic301144j | *Inorg. Chem.* 2012, 51, 9005−9016

Table 1. Crystal and Structure Refinement Data for $Ln_{0.5}Ln'_{0.5}(H_2O)_5[W(CN)_8]$ (where Ln/Ln′ = Eu^{3+}/Tb^{3+}, Eu^{3+}/Gd^{3+}, Tb^{3+}/Sm^{3+})

	Eu^{3+}/Tb^{3+}	Eu^{3+}/Gd^{3+}	Tb^{3+}/Sm^{3+}
formula	$C_{16}H_{20}EuN_{16}O_{10}TbW_2$	$C_{16}H_{20}EuGdN_{16}O_{10}W_2$	$C_{16}H_{20}N_{16}O_{10}smtbw_2$
formula weight	1275.06	1273.39	1273.45
crystal system	tetragonal	tetragonal	tetragonal
space group	*P*4/*nmm*	*P*4/*nmm*	*P*4/*nmm*
temperature (K)	150(2)	173(2)	173(2)
a,*b* (Å)	10.95080(10)	10.95220(10)	10.92020(10)
c (Å)	7.11970(10)	7.13630(10)	7.16970(10)
volume (Å^3)	853.795(16)	856.004(16)	854.992(16)
Z	1	1	1
D_c (g cm^{-3})	2.480	2.470	2.473
μ(Mo−Kα) (mm^{-1})	10.639	10.483	10.507
crystal size (mm)	0.24 × 0.18 × 0.16	0.16 × 0.16 × 0.10	0.11 × 0.10 × 0.07
crystal type	orange prisms	yellow prisms	yellow prisms
θ range	3.72 to 36.27	3.72 to 34.81	3.73 to 34.81
index ranges	$-18 \le h \le 17$	$-17 \le h \le 17$	$-17 \le h \le 17$
	$-18 \le k \le 18$	$-16 \le k \le 17$	$-17 \le k \le 17$
	$-11 \le l \le 11$	$-11 \le l \le 11$	$-11 \le l \le 11$
reflections collected	22394	29637	27331
independent reflections	1176 (R_{int} = 0.0258)	1058 (R_{int} = 0.0344)	1055 (R_{int} = 0.0294)
data completeness	up to θ = 36.27° 99.7%	up to θ = 34.81° 98.9%	up to θ = 34.81° 98.7%
final *R* indices [I > 2σ(I)][a,b]	*R*1 = 0.0138	*R*1 = 0.0144	*R*1 = 0.0129
	*wR*2 = 0.0326	*wR*2 = 0.0330	*wR*2 = 0.0292
final *R* indices (all data)[a,b]	*R*1 = 0.0139	*R*1 = 0.0169	*R*1 = 0.0155
	*wR*2 = 0.0326	*wR*2 = 0.0333	*wR*2 = 0.0295
weighting scheme[c]	*m* = 0.0083	*m* = 0.0163	*m* = 0.0155
	n = 1.7356	*n* = 0.3094	*n* = 0.2067
largest diff. peak and hole	1.816 and −4.536 eÅ^{-3}	0.501 and −1.758 eÅ^{-3}	0.908 and −0.984 eÅ^{-3}
CCDC number	753631	753632	753635

the visible region. However, only two compounds, $Tb(H_2O)_5[Mo(CN)_8]$ and $Tb(H_2O)_5[W(CN)_8]$, present both the characteristic Tb^{3+} luminescence and a clearly visible long-range magnetic ordering and thus may be considered as one of the first bifunctional magneto-luminescent molecule-based materials. These results encouraged us to pursue our effort in the synthesis of bifunctional luminescent molecule-based magnets by extending this approach to the association of different mixed luminescent (Eu^{3+}, Tb^{3+}) and paramagnetic lanthanides (Gd^{3+}, Sm^{3+}) combined with octacyanotungstate(V) building block. This strategy should ensure the presence of both magnetic and luminescent properties. Especially, for Tb^{3+}/Eu^3 cyano-bridged coordination polymers as the energy levels of the ions match perfectly, Tb^{3+}-to-Eu^{3+} energy transfer is highly efficient and should be favored over Tb^{3+} light emitting decay. Moreover, weak back energy transfer from Eu^{3+}-to-Tb^{3+} is also expected.[13]

In this Article, we report the synthesis, structure characterization, and investigation of luminescent and magnetic properties of three new two-dimensional lanthanide-mixed cyano-bridged coordination polymers $Ln_{0.5}Ln'_{0.5}(H_2O)_5[W(CN)_8]$ (where Ln/Ln′ = Eu^{3+}/Tb^{3+}, Eu^{3+}/Gd^{3+}, and Tb^{3+}/Sm^{3+}). These compounds present both, low-temperature magnetic transitions and luminescence and may be considered as bifunctional. A special emphasis was paid to the study of their luminescent properties and investigation of Tb^{3+}-to-Eu^{3+} energy transfer which depends on the excitation. This allowed modulating the color of luminescence through the tuning of the excitation band in order to design a multicolored light emitter.

2. RESULTS AND DISCUSSION

2. 1. Synthesis and Crystal Structures. The slow diffusion of diethyl ether into a 0.1 M solution of $[(N(C_4H_9)_4]_3[W(CN)_8]\cdot 2H_2O$ with a mixture of two 0.18 M solutions of $[Ln(H_2O)_5](NO_3)_3$ (Ln = Eu^{3+}, Tb^{3+}) and $[Ln'(H_2O)_6](NO_3)_3$ (Ln′ = Tb^{3+}, Gd^{3+}, Sm^{3+}) in acetonitrile led to the isolation of large amounts of single-crystal phases. Isolated compounds were fully characterized by elemental analyzes, FT-IR spectroscopy, and X-ray diffraction on single-crystal (Table 1). FT-IR C−N stretches for all compounds are shifted toward higher frequencies (2178−2180 cm^{-1}) over those of the parent $[(N(C_4H_9)_4]_3[W(CN)_8]\cdot 2H_2O$ compound (2141 (s), 2131, 2108 (s) cm^{-1}), thus confirming coordination of cyanide groups to Ln^{3+} and Ln'^{3+}. The presence of a ν(C−N) stretch in the 2120−2130 cm^{-1} range also suggests the existence of cyanide moieties, as confirmed unequivocally by structural studies detailed in the following paragraphs.

Single-crystal X-ray diffraction at low temperatures of 150 and 173 K reveals that all materials are identical, $Ln_{0.5}Ln'_{0.5}(H_2O)_5[W(CN)_8]$ (where Ln/Ln′ = Eu^{3+}/Tb^{3+}, Eu^{3+}/Gd^{3+}, and Tb^{3+}/Sm^{3+}), crystallizing in the tetragonal *P*4/*nmm* space group (Table 1). Because all materials are isotypical, the subsequent structural discussion will be mainly focused on $Eu_{0.5}Tb_{0.5}(H_2O)_5[W(CN)_8]$. Table 2 summarizes the main bond lengths for the $\{Ln_{0.5}Ln'_{0.5}N_4O_5\}$ and $\{WC_8\}$ coordination environments for all materials.

The crystal structures of aforementioned materials are composed of two crystallographically independent metallic centers, one for the rare-earth element and another for W^{5+}. Due to the very similar electronic densities associated with the

dx.doi.org/10.1021/ic301144j | Inorg. Chem. 2012, 51, 9005−9016

Table 2. Selected Bond Lengths (in Å) for the $\{Ln_{0.5}Ln'_{0.5}N_4O_5\}$ and $\{WC_8\}$ Coordination Environments Present in $Ln_{0.5}Ln'_{0.5}(H_2O)_5[W(CN)_8]$ (Where Ln/Ln′ = Eu^{3+}/Tb^{3+}, Eu^{3+}/Gd^{3+}, Tb^{3+}/Sm^{3+})

	Eu^{3+}/Tb^{3+}	Eu^{3+}/Gd^{3+}	Tb^{3+}/Sm^{3+}
$Ln_{0.5}Ln'_{0.5}(1)$–O(1W)	2.518(4)	2.528(4)	2.531(4)
$Ln_{0.5}Ln'_{0.5}(1)$–O(2W)	2.477(5)	2.431(9)	2.425(9)
$Ln_{0.5}Ln'_{0.5}(1)$–O(3W)	2.398(6)	2.479(6)	2.476(6)
$Ln_{0.5}Ln'_{0.5}(1)$–N(1)	2.507(3)	2.521(3)	2.507(3)
W(1)–C(1)	2.150(3)	2.148(4)	2.151(3)
W(1)–C(2)	2.153(3)	2.154(3)	2.155(3)

lanthanide centers, it was not possible to model from unrestrained refinements the rates of occupancy for each $Ln_{0.5}Ln'_{0.5}$ pair composing the $\{LnLn'N_4O_5\}$ coordination environments of the three studied materials. It was then assumed that each crystallographic location would be equally occupied by the lanthanide centers employed in the synthesis of the materials. As previously described by us for the isotypical $Ln(H_2O)_5[M(CN)_8]$ system (where Ln = Sm^{3+}, Eu^{3+}, Gd^{3+} or Tb^{3+}, and M = Mo^{5+} or W^{5+}),[10] the two crystallographic independent metallic coordination environments, $\{Ln_{0.5}Ln'_{0.5}N_4O_5\}$ and $\{WC_8\}$, are extensively affected by positional disorder (details on the refinement strategy are given in the Experimental Section dedicated to the crystallographic studies). Besides the coordination of O(1W) to $Ln_{0.5}Ln'_{0.5}$ all positions are, at least, split into two giving rise to a distribution of possible coordination spheres as depicted in Figure 1. Nevertheless, taking into consideration average locations for each disordered donor atom composing the coordination spheres, regular polyhedra can then be derived. The coordination sphere of the lanthanide centers can be envisaged as composed of four bridging cyanide groups and five water molecules, $\{Ln_{0.5}Ln'_{0.5}N_4O_5\}$, overall describing a slightly distorted tricapped trigonal prismatic coordination environment with the $Ln_{0.5}Ln'_{0.5}$–(N,O) bond lengths ranging from 2.391(5) to 2.531(4) Å for three studied compounds (Figure 1a and Table 2). We note that the $\{Ln_{0.5}Ln'_{0.5}N_4O_5\}$ coordination polyhedron can also be seen as a distorted square antiprism for which one of the basal planes is composed solely of water molecules while the other of cyanide ligands; the well-located O(1W) water molecule caps this latter basal plane (see Figure 1a). W(1) is instead coordinated to a total of eight cyanide ligands, with the $\{WC_8\}$ coordination geometry strongly resembling a slightly distorted dodecahedron (Figure 1b), which is typical of one-, two-, and three-dimensional coordination polymers containing $[W(CN)_8]^{3-}$ units. The registered W–C bond lengths fall within a very short-range, 2.148(4)–2.155(3) Å (Table 2), and are in good agreement with those typically observed in related compounds.[10,14]

Interpolyhedra connectivity is achieved by way of the μ_2-cyanide bridges [C(1)≡N(1)], leading to the formation of neutral two-dimensional $_\infty^2[Ln_{0.5}Ln'_{0.5}(H_2O)_5W(CN)_8]$ corrugated layers placed in the *ab* crystallographic plane as depicted in Figure 2a. For $Eu_{0.5}Tb_{0.5}(H_2O)_5[W(CN)_8]$, the shortest $Eu_{0.5}Tb_{0.5}(1)\cdots W(1)$ intermetallic distance is 5.7734(1) Å, which occurs along the plane of the two-dimensional layer, with the analogous interlayer distance being *ca.* 32% longer [7.6126(2) Å]. A note worth of mentioning for all structures is that the shortest $Ln_{0.5}Ln'_{0.5}(1)\cdots Ln_{0.5}Ln'_{0.5}(1)$ and $W(1)\cdots W(1)$ intermetallic distances always occur between adjacent layers, being of the magnitude of the length of the *c*-axis (see Table 1 for geometrical data). Connections between layers are ensured by strong O–H···N hydrogen bonds linking the coordinated molecules from one layer to the terminal (and disordered) C–N cyanide groups from the layer that is immediately adjacent (not shown).

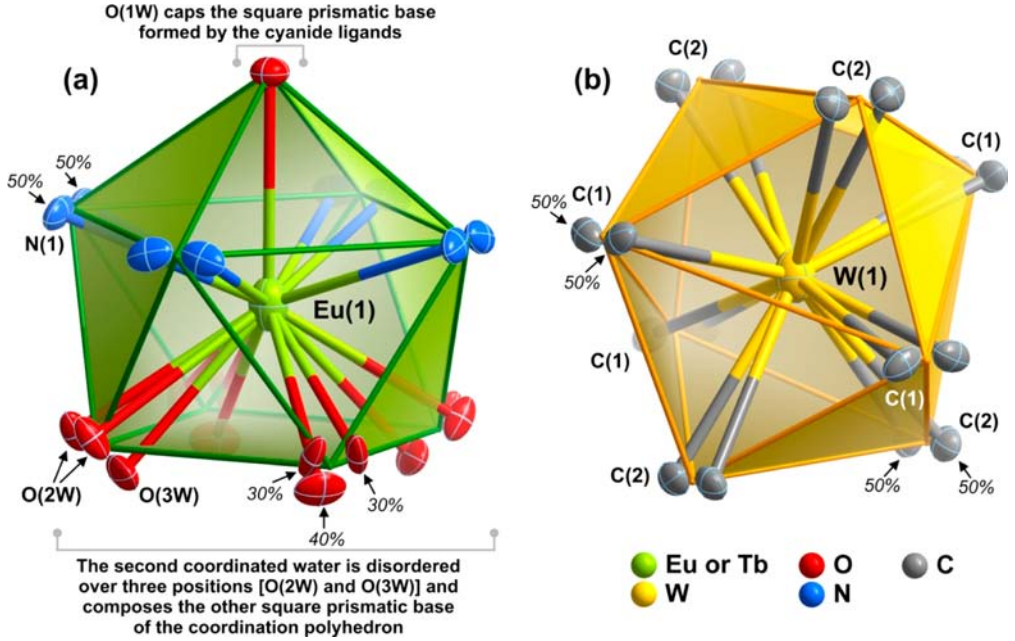

Figure 1. (a) Distorted tricapped trigonal prismatic $\{Eu_{0.5}Tb_{0.5}'N_4O_5\}$ and (b) distorted dodecahedral $\{WC_8\}$ coordination environments of the metallic centers composing the crystal structure of $Eu_{0.5}Tb_{0.5}(H_2O)_5[W(CN)_8]$. *Please note*: for simplicity only the presence of Eu(1) is indicated; in fact, the site is equally occupied by Eu^{3+} and Tb^{3+}. Atomic labels and individual rates of occupancy for all atoms composing the first coordination spheres are provided. Atoms from the cyanide and water molecules are represented as thermal ellipsoids drawn at the 30% probability level, while the metallic centers are instead represented as ellipsoids with 90% probability. Symmetry operations used to generate equivalent atoms have been omitted for clarity purposes. See Table 2 for tabulated bond lengths.

dx.doi.org/10.1021/ic301144j | *Inorg. Chem.* 2012, 51, 9005–9016

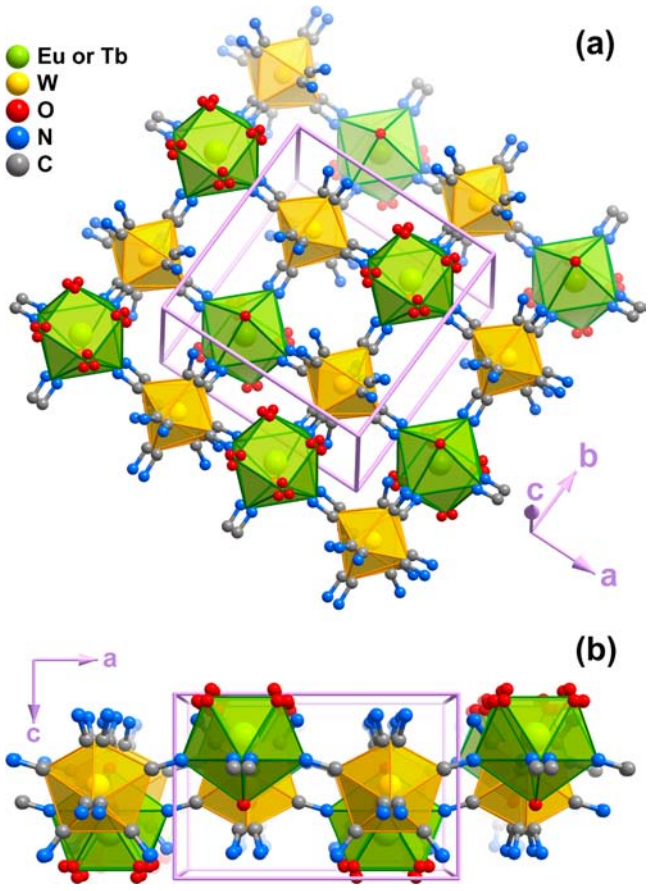

Figure 2. Perspective views of the neutral two-dimensional $_{\infty}^{2}[Eu_{0.5}Tb_{0.5}(H_2O)_5W(CN)_8]$ corrugated layers composing the crystal structure of $Eu_{0.5}Tb_{0.5}(H_2O)_5[W(CN)_8]$. The drawings emphasize the statistical positional disorder associated with all cyanide groups and most of the coordinated water molecules.

2.2. Photoluminescence Measurements. Figure 3 shows the room temperature emission spectra of $Eu_{0.5}Tb_{0.5}(H_2O)_5[W(CN)_8]$, $Eu_{0.5}Gd_{0.5}(H_2O)_5[W(CN)_8]$, and $Tb_{0.5}Sm_{0.5}(H_2O)_5[W(CN)_8]$ crystals excited at 280 and 350 nm. The spectra present the $^5D_4 \rightarrow {}^7F_{6-2}$ (Tb^{3+}) and $^5D_0 \rightarrow {}^7F_{0-4}$ (Eu^{3+}) intra-4*f* transitions. Sm^{3+} emission is not discerned.

For the Eu^{3+}-containing mixed-lanthanide compounds, $Eu_{0.5}Tb_{0.5}(H_2O)_5[W(CN)_8]$ and $Eu_{0.5}Gd_{0.5}(H_2O)_5[W(CN)_8]$, the energy and full width at half-maximum (fwhm) of the single $^5D_0 \rightarrow {}^7F_0$ line and of the Stark components of the $^5D_0 \rightarrow {}^7F_{1-2}$ transitions, resemble those observed for the emission spectra of the Eu^{3+} single-doped crystal $Eu(H_2O)_5[W(CN)_8]$.[10b] These results are in close agreement with the crystallographic studies which indicate an isotypical material for the single-doped and mixed cyano-bridged coordination polymers.

Figure 4a compares the room temperature excitation spectra of the $Tb_{0.5}Sm_{0.5}(H_2O)_5[W(CN)_8]$ and $Eu_{0.5}Tb_{0.5}(H_2O)_5[W(CN)_8]$ compounds monitored at 544 nm (Tb^{3+}, $^5D_4 \rightarrow {}^7F_5$ transition). All spectra reveal a low-relative intensity band in the 250−310 nm region attributed to the overlap between the spin-forbidden (high-spin, HS) interconfigurational *f*-*d* transition and the W-related ligand-to-metal-charge (LMCT) band,[10b,15] being dominated by the intra-4*f* [8] lines, ascribed to the $^7F_6 \rightarrow {}^5D_{4,3}$, $^5G_{6-4}$, $^5L_{10,9}$ transitions.

Figure 4b shows the excitation spectra of the $Eu_{0.5}Gd_{0.5}(H_2O)_5[W(CN)_8]$ and $Eu_{0.5}Tb_{0.5}(H_2O)_5[W(CN)_8]$ crystals

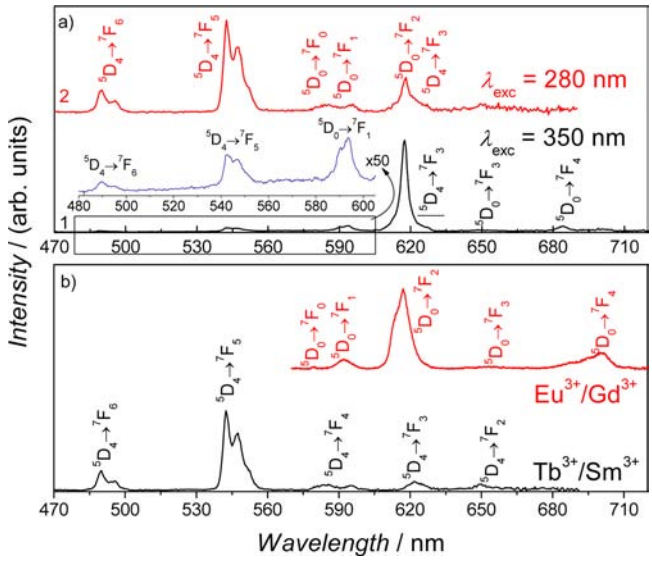

Figure 3. a) Room temperature emission spectra of $Eu_{0.5}Tb_{0.5}(H_2O)_5[W(CN)_8]$ excited at (1) 350 nm (black) and (2) 280 nm (red). The inset shows a magnification of the 480−605 nm spectral region. b) Room temperature emission spectra of $Eu_{0.5}Gd_{0.5}(H_2O)_5[W(CN)_8]$ (top, red) and $Tb_{0.5}Sm_{0.5}(H_2O)_5[W(CN)_8]$ (bottom, black) excited at 350 nm.

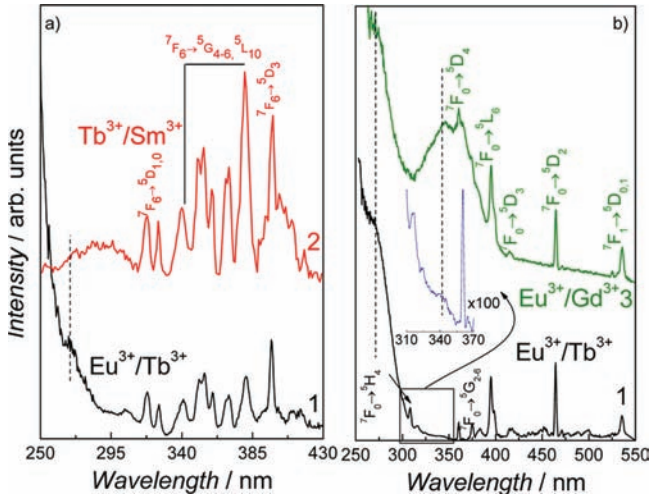

Figure 4. Room temperature excitation spectra of (1) $Eu_{0.5}Tb_{0.5}(H_2O)_5[W(CN)_8]$ (black), (2) $Tb_{0.5}Sm_{0.5}(H_2O)_5[W(CN)_8]$ (red), and (3) $Eu_{0.5}Gd_{0.5}(H_2O)_5[W(CN)_8]$ (green) crystals monitored at a) 544 nm and b) 618 nm. The inset shows a magnification of the excitation spectrum of $Eu_{0.5}Tb_{0.5}(H_2O)_5[W(CN)_8]$ crystals in the O→W LMCT band (310−370 nm). The dash lines assign LMCT transitions.

displaying the typical intra-4*f*^{6} $^7F_{0,1} \rightarrow {}^5D_{4,2,1}$, $^5G_{2-4}$, $^5L_6$ transitions and two broad bands centered at around 260 and 350 nm ascribed to the LMCT states. It is difficult to unequivocally identify the precise nature of the LMCT transitions as they can be ascribed either to O→W (at 260 nm, since strong H-bonds exist between the terminal cyano moieties and the water molecules) and O→Eu^{3+}[10b] or cyano→W^{14} transitions (at 350 nm). Contrarily to that found for the single-doped $Eu(H_2O)_5[W(CN)_8]$ compound,[10b] the main excitation path for the Eu^{3+} ions in the $Eu_{0.5}Gd_{0.5}(H_2O)_5[W(CN)_8]$ and $Eu_{0.5}Tb_{0.5}(H_2O)_5[W(CN)_8]$ materials is *via* the LMCT states, rather than direct intra-4*f*. The absence of Gd^{3+} and Tb^{3+} excited states in the excitation spectra

dx.doi.org/10.1021/ic301144j | *Inorg. Chem.* 2012, 51, 9005−9016

of the $Eu_{0.5}Gd_{0.5}(H_2O)_4[W(CN)_8]$ and $Eu_{0.5}Tb_{0.5}(H_2O)_5[W(CN)_8]$ monitored within the Eu^{3+} transitions, respectively, points out the absence, at room temperature, of $Gd^{3+} \rightarrow Eu^{3+}$ and $Tb^{3+} \rightarrow Eu^{3+}$ efficient energy transfer, respectively.

The existence of Tb^{3+}-to-Eu^{3+} energy transfer was investigated by studying the photoluminescence features of the $Eu_{0.5}Tb_{0.5}(H_2O)_5[W(CN)_8]$ crystals at 14 K. At this temperature, the signal-to-noise intensity ratio is favored permitting therefore a detailed study. Figure 5 shows the excitation spectra monitored

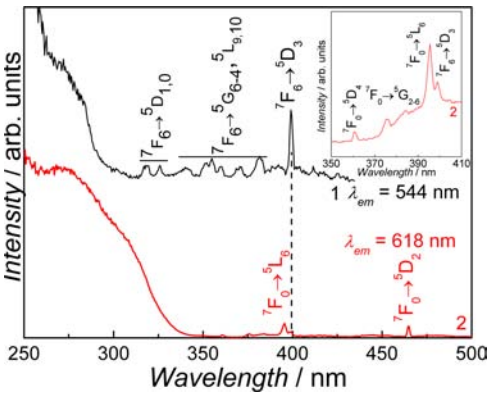

Figure 5. Excitation spectra acquired at 14 K for the $Eu_{0.5}Tb_{0.5}(H_2O)_5[W(CN)_8]$ crystal monitored at (1) 544 nm (black) and (2) 618 nm (red). The inset shows a magnification in order to evidence the presence of the intra4f^8 lines ($^7F_6 \rightarrow {}^5D_3$) in the excitation spectrum monitored at 618 nm.

within the $Eu^{3+}{}^5D_0 \rightarrow {}^7F_2$ transition (618 nm). The presence of Tb^{3+}-to-Eu^{3+} energy transfer at 14 K is clearly evidenced by the presence of the $^7F_6 \rightarrow {}^5D_3$ intra-4*f* Tb^{3+} lines in the excitation spectrum of $Eu_{0.5}Tb_{0.5}(H_2O)_5[W(CN)_8]$ monitored within the $Eu^{3+}{}^5D_0 \rightarrow {}^7F_2$ transition (inset Figure 5). Furthermore, the existence of Tb^{3+}-to-Eu^{3+} energy transfer indicates that no phase separation between lanthanide ions occurs, pointing out a uniform distribution within the lanthanide mixed compounds. The low-temperature emission features (Figure 1S, Electronic Supporting Information (ESI)) resemble those acquired at room temperature (Figure 3). As a result, whatever the excitation wavelength (280 or 350 nm) and the temperature experiment, both luminescence of Eu^{3+} and Tb^{3+} are observed. The only change concerns a slight modification in the relative emission intensities.

During the photoluminescence studies at 10 K and at room temperature within the excitation wavelength range 280−350 nm, all the codoped crystals become dark brown after continuous illumination (*cw*) as illustrated in Figure 6 for the $Eu_{0.5}Tb_{0.5}(H_2O)_5[W(CN)_8]$ crystal. The effect of the darkness of the crystals on the emission spectra is exemplified in Figure 6a, revealing that whereas the energy and fwhm of the Tb^{3+}- and Eu^{3+}-related emissions remain unaltered, their corresponding relative intensities strongly depend on the irradiation time. In particular, the emission intensity of the Tb^{3+} lines remains approximately constant, and the intensity of the Eu^{3+}- related transitions increases as the irradiation time increases. Note also that compounds $Eu(H_2O)_5[W(CN)_8]$ or $Tb(H_2O)_5[W(CN)_8]$ do not show similar light induced transformations.

2. 3. Magnetic Properties. The paramagnetic lanthanide ions Eu^{3+}, Tb^{3+}, and Sm^{3+} constituting the $Ln_{0.5}Ln'_{0.5}(H_2O)_5[W(CN)_8]$ coordination polymers exhibit a first-order angular momentum, and only Gd^{3+} ion (f^7 configuration) presents an orbitally nondegenerate ground state. For the $4f^n$ configuration

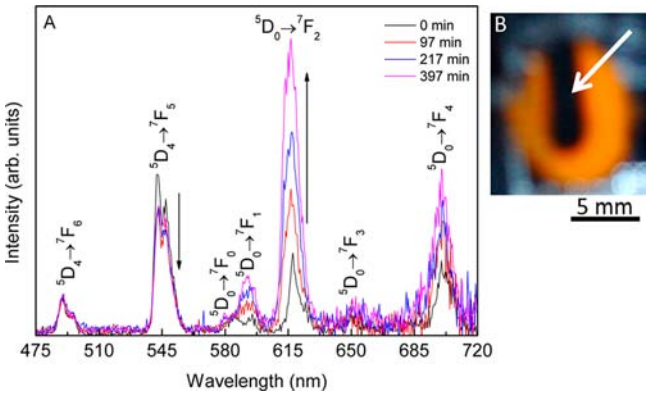

Figure 6. a) Emission spectra acquired at 300 K for the $Eu_{0.5}Tb_{0.5}(H_2O)_5[W(CN)_8]$ crystals as function of *cw* irradiation time. The excitation and irradiation wavelength was 350 nm. b) Photograph of an ensemble of crystals. The arrow indicates the black region resulting after 10 min of irradiation.

of a Ln^{3+} ion, it splits into $^{2S+1}L_J$ states by interelectronic repulsion and spin−orbit coupling. Further splitting into Stark sublevels is caused by crystal-field perturbation (up to $2J+1$ if n is even and $J+1/2$ if n is odd). The number of Stark sublevels depends on the site symmetry of the lanthanide ion. For all magnetic Ln^{3+}, except Sm^{3+}, the $^{2S+1}L_J$ ground state is well separated in energy from the first excited states. At high temperature, all Stark levels arising from this ground state are populated, but as the temperature decreases the effective magnetic moment of the lanthanide ions will change by thermal depopulation of the Stark sublevels. As a result, temperature dependence of the (de)population of the Stark levels of lanthanide ions leads to a deviation of the magnetic susceptibility with respect to the Curie law. When a lanthanide ion is involved in the interaction with transition metal ions, this phenomenon and the magnetic interactions with transition metal ions should be taken into account. The sum of these effects creates great difficulties in understanding the magnetic properties of lanthanide-containing compounds. In $Ln_{0.5}Ln'_{0.5}(H_2O)_5[W(CN)_8]$ compounds, the 5*d* transition metal ion W^{5+} having $S = 1/2$ and $g = 2$ is linked through cyano ligands with two different lanthanide ions. While the exact localization of the lanthanides is well-defined, we can postulate either their random distribution as {-Ln-NC-W-CN-Ln′-} linkages on the base of photoluminescent results showing the presence of Tb^{3+} to Eu^{3+} energy transfer which clearly indicates the close proximity of two rare-earth ions.

$Eu_{0.5}Tb_{0.5}(H_2O)_5[W(CN)_8]$. This compound contains two paramagnetic lanthanide ions Eu^{3+} and Tb^{3+} interacting with the paramagnetic ion W^{5+} giving rise to two possible types of interactions through the cyano bridge: Eu^{3+}-NC-W^{5+} and Tb^{3+}-NC-W^{5+}. On the one hand, Eu^{3+} has a nonmagnetic $^7F_0$ ground state with the first excited state $^7F_1$ at *ca.* 350 cm^{-1} and $^7F_2$ at *ca.* 1000 cm^{-1}.[16] At room temperature these excited states are populated, but as the temperature decreases, there is a progressive depopulation of the excited doublets. At low temperature only the nonmagnetic ground level is occupied. In this case, the susceptibility of the isolated ion becomes temperature independent due to field-determined admixing of the excited states into $^7F_0$. On the other hand, Tb^{3+} has a $^7F_6$ ground state with a first-order orbital momentum. In a low symmetry site, this state is split into Stark components by the crystal field, each of them being a Kramers doublet. As the temperature is lowered, the highest energy Kramers doublets are progressively depopulated, leading to a pronounced deviation of the magnetic behavior with respect to the Curie law.

dx.doi.org/10.1021/ic301144j | *Inorg. Chem.* 2012, 51, 9005−9016

The temperature dependence of χT performed for this compound with an applied field of 1000 Oe is shown in Figure 7.

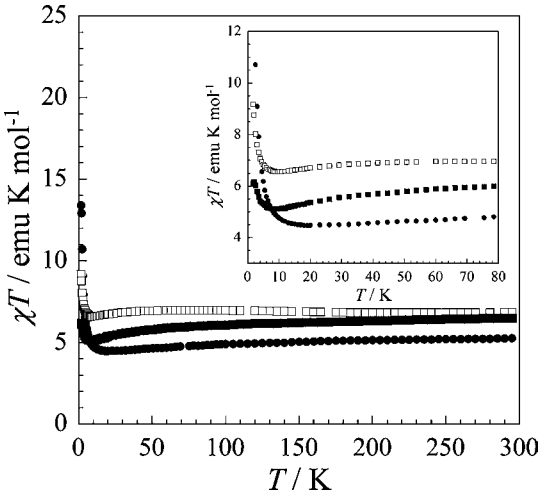

Figure 7. Temperature dependence of χT performed for $Eu_{0.5}Tb_{0.5}(H_2O)_5[W(CN)_8]$ (■), $Eu_{0.5}Gd_{0.5}(H_2O)_5[W(CN)_8]$ (●), and $Tb_{0.5}Sm_{0.5}(H_2O)_5[W(CN)_8]$ (□) with an applied field of 1000 Oe.

At 300 K, the χT value is equal to 6.50 emu K mol^{-1} that corresponds to the one calculated of 7.00 emu K mol^{-1} for a noninteracting 1/2·Eu^{3+} (1/2●1.5 emu K mol^{-1}), 1/2·Tb^{3+} (1/2●11.75 emu K mol^{-1}) ions and one W^{5+} ion (0.375 emu K mol^{-1}).[17] The χT curve decreases slowly as the temperature decreases, reaches a minimum at 9.16 K (χT = 5.11 emu K mol^{-1}), and increases abruptly after that. The decrease of this curve with temperature may be explained by the depopulation of the excited states $^7F_1$, $^7F_2$ of Eu^{3+} and the Stark levels of the terbium $^7F_6$ ground state. At lower temperature, only the nonmagnetic ground level of Eu^{3+} is occupied, and the magnetic behavior of this compound may be determined only by taking into account the exchange interactions between the Tb^{3+} and W^{5+}. The presence of a minimum on this curve may thus be attributed to the depopulation of the Stark levels of the terbium $^7F_6$ ground state as the temperature is lowered. Note that the temperature dependence of χT performed for $Tb(H_2O)_5[W(CN)_8]$ presents a similar behavior at low temperature. In both cases, the increase of χT at low temperature is due to ferromagnetic correlations between Tb^{3+} and W^{5+}.

The field dependence of the magnetization performed at 2 K shows that the magnetization increases rapidly with an applied magnetic field, and the value of the magnetization at 50 kOe is equal to 3.39 μ_B (Figure 8). Assuming that at this temperature Eu^{3+} is not magnetic, only the interactions between Tb^{3+} and W^{5+} and weak interactions between two W^{5+} through nonmagnetic Eu^{3+} are operational. The observed value corresponds well to the presence of ferromagnetic interactions between the Tb^{3+} and W^{5+} ions (3.50 μ_B) if we assume a spin of S_W = 1/2 with g = 2 for W^{5+} ion and take into account the approximation of an effective spin S = 1/2 with strong uniaxial Ising-spin anisotropy of the g tensor, $g_{\parallel}$ = 10 and $g_{\perp}$ = 0 for the Tb^{3+} ion.[10a,b,11,18] The presence of ferromagnetic Tb^{3+}-W^{5+} interactions through the cyano bridge is in good agreement with what has been previously reported for $Tb(H_2O)_5[W(CN)_8]$.[10a,b]

The magnetic properties of this compound were investigated with alternative current (ac) measurements. The temperature dependence of the in-phase, χ', and out-of-phase, χ'', ac

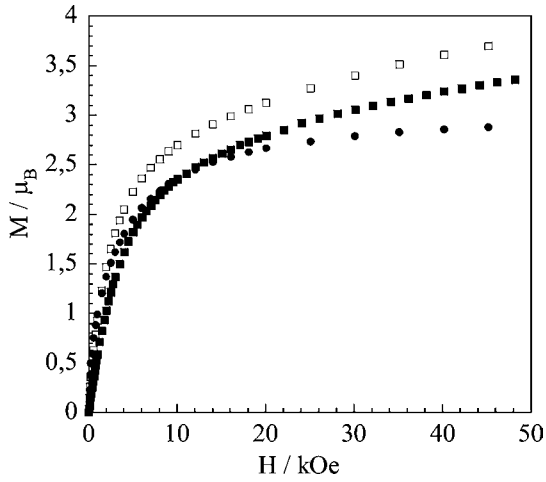

Figure 8. Field dependence of the magnetization performed for $Eu_{0.5}Tb_{0.5}(H_2O)_5[W(CN)_8]$ (■), $Eu_{0.5}Gd_{0.5}(H_2O)_5[W(CN)_8]$ (●), and $Tb_{0.5}Sm_{0.5}(H_2O)_5[W(CN)_8]$ (□) at 1.8 K.

susceptibility components for $Eu_{0.5}Tb_{0.5}(H_2O)_5[W(CN)_8]$ in zero applied direct current (dc) field was performed at different frequencies varying between 1 and 1488 Hz. As temperature decreases, the χ' curves increase abruptly after 3 K, while the χ'' curves increase sharply after 2.5 K showing frequency dependent peaks (Figure 9). Usually, the frequency independence of the ac

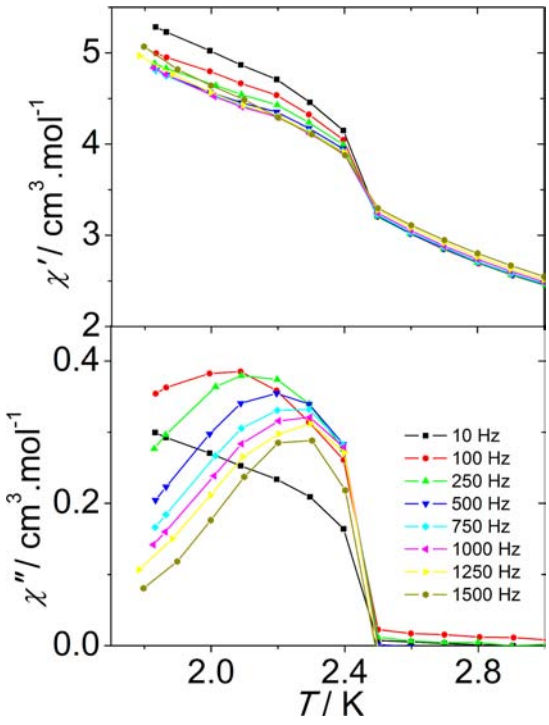

Figure 9. Temperature dependences of in-phase, χ', (top) and out-of phase, χ'', (bottom) components of the ac susceptibility performed with different frequencies for $Eu_{0.5}Tb_{0.5}(H_2O)_5[W(CN)_8]$.

susceptibility peaks suggests the presence of a long-range magnetic ordering, while the frequency dependence indicates the presence of a short-range ordering. The temperature dependence of the relaxation time extracted from the maximum of the χ'' component of the ac susceptibility was fitted with the conventional critical scaling law of the spin dynamics, $\tau = \tau_0[T_g/(T_{max}-T_g)]^{zv}$,

dx.doi.org/10.1021/ic301144j | Inorg. Chem. 2012, 51, 9005−9016

where T_g is the glass temperature and $z\nu$ is a critical exponent.[19] The best fits give T_g = 1.7 K, $\tau_0 = 3.5 \times 10^{-8}$ s, and $z\nu$ = 5.4 (Figure 2S, ESI). The obtained $z\nu$ and τ_0 values are in the range 4−12 and 10^{-8}−10^{-12} s, respectively, expected for classical spin glass systems.[15] It is interesting to note that for the pure compound $Tb(H_2O)_5[W(CN)_8]$ both χ' and χ'' responses are not frequency dependent, indicating the presence of a long-range magnetic ordering below 2.8 K. In the case of $Eu_{0.5}Tb_{0.5}(H_2O)_5[W(CN)_8]$ this frequency dependence may be explained by the presence of Tb^{3+}-NC-W^{5+} domains existing even in the case of a random lanthanide distribution separated by diamagnetic -CN-Eu^{3+}-NC- bridges that break the propagation of the Tb^{3+}-NC-W^{5+} interactions at long distances and leads to the appearance of a short-range magnetic ordering.

$Eu_{0.5}Gd_{0.5}(H_2O)_5[W(CN)_8]$. This compound presents two types of exchange interactions through the cyano bridge: Eu^{3+}-NC-W^{5+} and Gd^{3+}-NC-W^{5+}. The Gd^{3+} ion has a $^8S_{7/2}$ ground state without first-order angular momentum.

The field dependence of the magnetization performed at 1.8 K (Figure 8) shows that the magnetization increases rapidly with an applied magnetic field, and the value of the magnetization at 50 kOe is equal to 2.91 μ_B. As in the previous case, at this temperature the Eu^{3+} is nonmagnetic, and only the Gd^{3+}-NC-W^{5+} interactions and weak interactions between two W^{5+} ions through nonmagnetic Eu^{3+} are operational. The value of the saturation magnetization calculated for antiferromagnetic Gd^{3+}-M^{5+} interactions is equal to 2.50 μ_B and for ferromagnetic Gd^{3+}-M^{5+} interactions is equal to 4.5 μ_B. The observed magnetization value rather indicates the presence of antiferromagnetic interactions between Gd^{3+} and W^{5+}. Note that antiferromagnetic interactions have also been found in the case of $Gd(H_2O)_5[W(CN)_8]$.[10b]

The temperature dependence of the χT product performed for $Eu_{0.5}Gd_{0.5}(H_2O)_5[W(CN)_8]$ with an applied field of 1000 Oe are shown in Figure 7. At 300 K, the χT value of 5.30 emu K mol^{-1} corresponds to that calculated (5.06 emu K mol^{-1}) for noninteracting 1/2·Eu^{3+} (1/2·1.50 emu K mol^{-1}), 1/2·Gd^{3+} with S = 7/2 with ground state $^8S_{7/2}$ (1/2·8.19 emu K mol^{-1}), and one W^{5+} (0.375 emu K mol^{-1}) ions. As the temperature decreases χT decreases progressively, reaching a minimum value at 18.56 K (χT = 4.47 emu K mol^{-1}), and then increases rapidly at low temperature. The presence of a minimum on this curve may be explained by the competition between depopulation of the excited states $^7F_1$, $^7F_2$ of Eu^{3+} and/or the occurrence of antiferromagnetic interactions between the Gd^{3+} and W^{5+} ions, both phenomena inducing a curve decrease with temperature. Note that a similar curve shape was also observed for the compound $Gd(H_2O)_5[W(CN)_8]$ with only Gd^{3+} ion which exhibits antiferromagnetic interactions between the spin carriers.[10b]

The temperature dependence of the ac susceptibility shows an abrupt increase of χ' and χ'' responses below 2.5 K (Figure 3S, ESI), indicating the beginning of a magnetic transition. However, due to the absence of a clear maximum it is difficult to determine the nature of this transition. Note also the appearance of a frequency-dependent behavior on these curves as it was observed for $Eu_{0.5}Tb_{0.5}(H_2O)_5[W(CN)_8]$.

$Sm_{0.5}Tb_{0.5}(H_2O)_5[W(CN)_8]$. The Sm^{3+} ion has a $^6H_{5/2}$ ground state, which splits by the spin−orbit coupling into six levels. The first ($^6H_{7/2}$) and even higher excited states can be populated at room temperature. As a consequence, the high-temperature behavior of χT *vs* T for the Sm^{3+} ion deviates from linearity. In addition, the presence of low-lying excited states adds a significant temperature independent contribution to the magnetic susceptibility. The temperature dependences of the χT product performed for $Sm_{0.5}Tb_{0.5}(H_2O)_5[W(CN)_8]$ with an applied magnetic field of 1000 Oe is shown in Figure 7. At 300 K the χT values are equal to 6.80 emu K mol^{-1} that is slightly higher than the expected value (6.29 emu K mol^{-1}) calculated for noninteracting 1/2·Sm^{3+} (1/2·0.89 emu K mol^{-1}), 1/2·Tb^{3+} (1/2·11.75 emu K mol^{-1}), and one W^{5+} (0.37 emu K mol^{-1}) ions.[13] The χT value slowly increases as the temperature decreases and then rapidly decreases below 50 K, reaches a minimum at 9.7 K (χT = 6.54 emu K mol^{-1}), and then increases rapidly at low temperature. The presence of a minimum on this curve may be attributed to the depopulation of the Stark levels for both the terbium and samarium ions. The field dependence of the magnetization performed at 1.8 K shows a magnetization value of 4.0 μ_B at 70 kOe (Figure 8) that corresponds to that calculated for Sm^{3+}-NC-W^{5+} and Tb^{3+}-NC-W^{5+} ferromagnetic interactions (3.9 μ_B). The temperature dependence of the ac susceptibility performed for $Sm_{0.5}Tb_{0.5}(H_2O)_5[W(CN)_8]$ shows that both χ' and χ'' responses increase abruptly at low temperature suggesting the presence of a magnetic transition, but no maximum was observed above 1.8 K (Figure 4S, ESI).

2. 4. Dependence of the Magnetic Properties According to UV Irradiation. As already observed for the photoluminescence measurements, the samples show peculiar behavior under UV irradiation: the crystals change color from orange to dark brown. In order to investigate this light induced transformation, we have focused our study on the compound $Eu_{0.5}Tb_{0.5}(H_2O)_5[W(CN)_8]$. First of all the structural transformations were checked by IR spectroscopy and X-ray diffraction on the irradiated sample. After irradiation at 355 nm for 15 min the IR spectrum of this compound shows modifications in the 2000−2300 cm^{-1} spectral window (cyanide region). The progressive vanishing of the band at 2150 cm^{-1} and the appearance of a broad band at 2123 cm^{-1} were observed (Figure 5S, ESI). This shift toward lower energy may suggest a progressive modification of the oxidation state of W^{5+} to W^{4+} resulting in an increase of π-back-donation, which shifts the CN stretching band toward lower frequency, as observed in the respective precursors.[20] However, no clear reversibility was observed after exposure of these crystals during few days to white light. Even after a short UV exposure, the crystals become dark brown as shown in Figure 6b. Nevertheless, this only occurs at the crystal surface: when one breaks the crystal it is possible to see that the interior retains the original color while the exterior is dark brown. The collection of single-crystal X-ray diffraction data on a crystal which was exposed for only a few minutes reveals that the structure did not change. This is in accordance with the fact that the modifications observed occur only at the crystal surface for short irradiation time. Consequently, for a crystal that has suffered from a longer exposure time (*i.e.*, more than 30 min of continuous irradiation) crystallinity was completely lost.

In order to confirm the change in the oxidation state of W^{5+} EPR experiments were also performed before and after UV irradiation. A complete vanishing of the signal at g = 1.968 characteristic of W^{5+} with S = 1/2 was observed in the EPR spectrum of this compound after 15 min of UV irradiation. This result confirms the hypothesis of the $W^{5+} \rightarrow W^{4+}$ transition after irradiation taking into account that W^{4+} gives no EPR signal due to its diamagnetic nature (Figure 6S, ESI). The investigation of the magnetic properties by SQUID magnetometry also confirms this electronic modification induced by UV irradiation (Figure 10).

The field dependence of the magnetization performed at 1.8 K before and after 15 min of UV irradiation shows that the value of the magnetization at 7 T for the irradiated sample is indeed lower (3.29 μ_B) compared to that for the nonirradiated sample (3.62 μ_B)

dx.doi.org/10.1021/ic301144j | *Inorg. Chem.* 2012, 51, 9005−9016

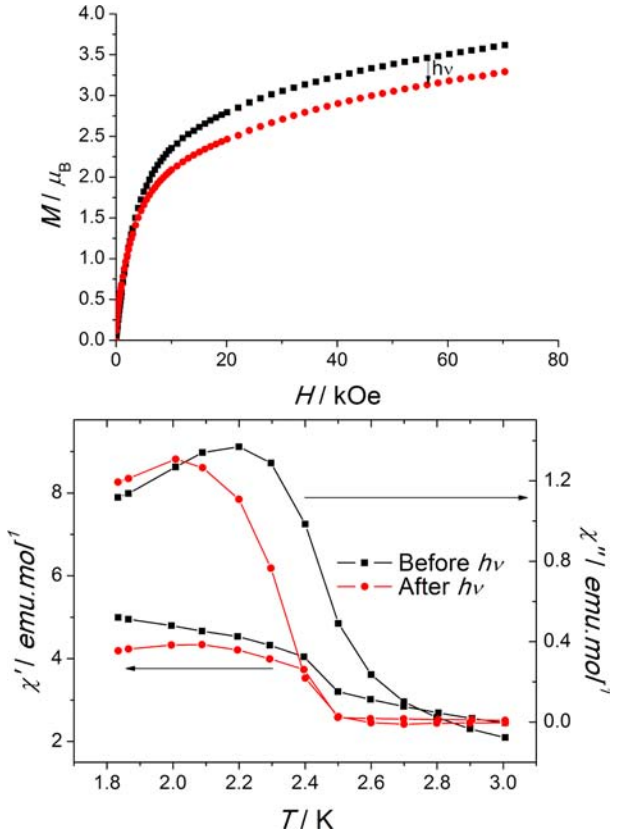

Figure 10. a) Field dependence of the magnetization for the nonirradiated (■) and irradiated (●, red) $Eu_{0.5}Tb_{0.5}(H_2O)_5[W(CN)_8]$. b) Temperature dependence of in-phase, χ', and out-of phase, χ'', components of the ac susceptibility performed at 999.87 Hz for the nonirradiated (■) and irradiated (●, red) $Eu_{0.5}Tb_{0.5}(H_2O)_5[W(CN)_8]$.

(Figure 10a). This supports a loss of spin caused by the appearance of the diamagnetic species $[W^{IV}(CN)_8]^{4-}$. The difference of the magnetization values (0.33 μ_B) compared to the theoretical one (1.00 μ_B), if 100% of the $[W^{V}(CN)_8]^{3-}$ complexes are photoreduced, can be ascribed to partial transformation of W^{5+} ions. The alternative current measurements also indicate a noticeable change in both χ' and χ'' temperature dependence where a clear shift toward lower temperature is observed (Figure 10b). It is important to point out that such degradation occurs only for the mixed compounds.

2.5. Computational Studies. In order to understand the light induced transformation which occurs for $Eu_{0.5}Tb_{0.5}(H_2O)_5[W(CN)_8]$ and not for nonmixed lanthanide-containing compounds $Eu(H_2O)_5[W(CN)_8]$ and $Tb(H_2O)_5[W(CN)_8]$, ground state periodic density functional theory (DFT) calculations were performed on these three compounds. The full optimization of the atomic positions in these crystals shows minimal difference that signifies similar structural atomic configuration.[10a,b] Nevertheless, some non-negligible differences exist between the optimized and the initial crystallographic positions. In the case of interatomic distances, differences of up to 0.16 Å are found for Ln−OH_2 distances, while the rest of bond lengths differ by less than 0.03 Å. Interestingly, the largest difference found for the Ln−OH_2 distances is calculated for O(1W) which is the least disordered of the water molecules in the crystallographic structure. Upon the optimization procedure, small changes are found between calculated and experimental angles. For instance, differences for Ln-W-Ln and W-Ln-W angles are smaller than 0.7°. The most important differences, of up to ~3°, are calculated for the atoms of the cyanide moieties.

The negligible structural differences between the three type of crystals, *i.e.*, $Ln(H_2O)_5[W(CN)_8]$ (Ln = Eu, Tb) and $Eu_{0.5}Tb_{0.5}(H_2O)_5[W(CN)_8]$, induce concomitant tiny differences on the calculated Bader charges, (Table 3). Thus, the largest deviations are found for Eu and W species in single-doped Eu and mixed Eu−Tb crystals with differences of only 0.07 *e* and 0.04 *e*.

Table 3. Calculated Bader Charges for $Eu_{0.5}Tb_{0.5}(H_2O)_5[W(CN)_8]$ and $Ln(H_2O)_5[W(CN)_8]$ ($Ln = Eu^{3+}$, Tb^{3+})

	Bader charge (a.u.)		
atom	$Eu(H_2O)_5[W(CN)_8]$	$Tb(H_2O)_5[W(CN)_8]$	$Eu_{0.5}Tb_{0.5}(H_2O)_5[W(CN)_8]$
Eu	2.05	——	2.12
Tb	——	2.35	2.34
W	2.59	2.65	2.63
C	1.91	1.91	1.90
N	−2.52	−2.51	−2.52
O(1W)	−1.98	−1.98	−1.97/−1.97
O(2W)	−2.00	−1.98	−1.99/−1.99
O(3W)	−2.00	−2.00	−1.98/−2.00

The calculated total density of states (DOS) for each atom are displayed in Figure 11. At first glance it seems that the DOS for all the atoms are almost the same for the three crystals with expected peak shifts for the DOS of the lanthanide ions. However, a deeper comparison (right column) shows that the positions of the peaks for the Tb^{3+} ion in the pure material and in the mixed crystal are the same (states are halved in the case of the mixed sample), while a different behavior is noticed for the Eu^{3+} ion in the pure and in the mixed materials. In the latter case, peak shifting between the two materials is found, which is followed by a small reorganization of the states in the oxygen atoms in regions close to −18 eV.

Thus, from the DFT results, the distinct light induced behavior observed for $Eu_{0.5}Tb_{0.5}(H_2O)_5[W(CN)_8]$ probably arises from the electronic rearrangement of Eu and O species when compared with the same atoms in $Eu(H_2O)_5[W(CN)_8]$.

3. CONCLUSION

In summary, we report here the synthesis, structure, and photoluminescent and magnetic properties for three new lanthanide-mixed cyano-bridged coordination polymers $Ln_{0.5}Ln'_{0.5}(H_2O)_5[W(CN)_8]$ (where Ln/Ln′ = Eu^{3+}/Tb^{3+}, Eu^{3+}/Gd^{3+}, and Tb^{3+}/Sm^{3+}). These compounds are isomorphous and crystallize in the tetragonal system *P*4/*nmm* forming two-dimensional grid-like networks. The photoluminescence measurements show that these compounds present the characteristic Tb^{3+} ($^5D_4 \rightarrow {}^7F_{6-2}$), Sm^{3+} ($^4G_{5/2} \rightarrow {}^6H_{7/2}$) and Eu^{3+} ($^5D_0 \rightarrow {}^7F_{0-4}$) intra 4f lines. Investigations on their magnetic properties demonstrate the presence of low temperature magnetic transitions with ferromagnetic Ln^{3+}-W^{5+} interactions in the case of Tb^{3+} and Sm^{3+} and antiferromagnetic ones for the Gd^{3+}-W^{5+} pair (except for Eu^{3+} ion that is not magnetic at low temperature). The presence of both, luminescence and magnetic transitions, suggests that these compounds may be identified as bifunctional coordination polymers with diverse physical responses when subjected to various external stimuli.

The main advantage of mixed lanthanide-containing compounds in comparison with those containing a single lanthanide is related to their photoluminescence. First, the introduction of an optically active lanthanide ion (Eu^{3+} or Tb^{3+}) to the magnetic

dx.doi.org/10.1021/ic301144j | *Inorg. Chem.* 2012, 51, 9005−9016

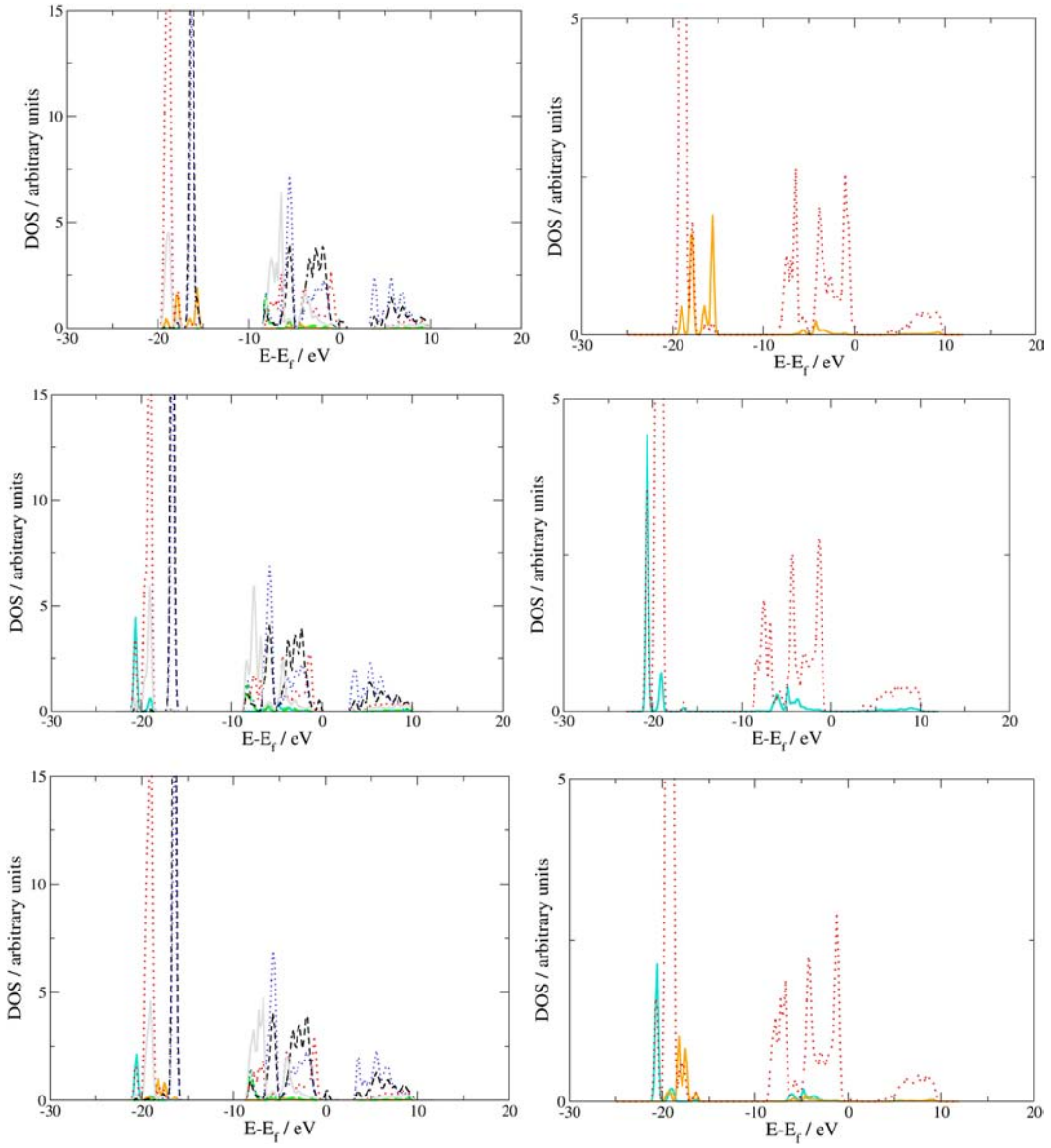

Figure 11. Calculated density of states (DOS) for $Eu(H_2O)_5[W(CN)_8]$ (top), $Tb(H_2O)_5[W(CN)_8]$ (middle), and $Eu_{0.5}Tb_{0.5}(H_2O)_5[W(CN)_8]$ (bottom) crystals. The left column shows DOS for all nuclei, while the right column shows a magnification of DOS for Ln and O atoms. Code color: turquoise is Tb; orange is Eu; green is W; black is C; blue is N; red is O; gray is H.

$Gd(H_2O)_5[W(CN)_8]$ or $Sm(H_2O)_5[W(CN)_8]$ coordination polymer networks provides bifunctionality (luminescence and magnetic properties). Second, the presence of two luminescent lanthanide ions within the same network (for instance Eu^{3+} and Tb^{3+}) offers the possibility of a bimodal (or a multicolored) emission. Along this line of thought, $Eu_{0.5}Tb_{0.5}(H_2O)_5[W(CN)_8]$ presents both green (Tb^{3+}) and red (Eu^{3+}) emission, and the emission color may be controlled by the excitation wavelength. Moreover, at low temperature (14 K), the excitation spectrum of the mixed $Eu_{0.5}Tb_{0.5}(H_2O)_5[W(CN)_8]$ coordination polymer monitored at the main Eu^{3+} emission (*ca.* 618 nm) clearly shows evidence of Tb^{3+}-to-Eu^{3+} energy transfer. Ion−ion energy transfer in solid state is a well-known phenomenon,[21] especially for hybrid materials when the localization of the two ions is close.[22] The process, which seems not to operate at room temperature, occurs through the cyanide ligands (exchange mechanism) or through space (multipolar mechanism).[21]

The magnetic properties of mixed lanthanides compounds exhibit a relatively small difference in comparison to the parent networks containing a single lanthanide ion. However a frequency dependence of the ac susceptibility associated with the presence of a short-range magnetic ordering was clearly observed for the mixed $Eu_{0.5}Tb_{0.5}(H_2O)_5[W(CN)_8]$ and $Eu_{0.5}Gd_{0.5}(H_2O)_5[W(CN)_8]$, while the related single lanthanide-containing compounds $Tb(H_2O)_5[W(CN)_8]$ and $Gd(H_2O)_5[W(CN)_8]$ present a long-range magnetic ordering without any frequency dependence of the ac susceptibility. Visibly, the introduction of a nonmagnetic Eu^{3+} ion breaks the propagation of the Ln^{3+}-NC-W^{5+} (Ln^{3+} = Tb, Gd) interactions at long distances leading to an appearance of the short-range magnetic ordering.

Another point to consider concerns the distribution of the two lanthanide ions, which may be randomly distributed or "aggregated" in the coordination polymer network. As mentioned above, the single-containing lanthanide and mixed lanthanide compounds present similar crystal structures, and the localization of two lanthanides cannot be performed crystallographically. However, several observations are in agreement with a random lanthanide

dx.doi.org/10.1021/ic301144j | *Inorg. Chem.* 2012, 51, 9005−9016

distribution: (i) The existence of a Tb^{3+}-to-Eu^{3+} energy transfer indicates the presence of relatively close distances between these ions pointing out their uniform distribution within the crystals. (ii) Just a slight decrease of the transition temperature observed for the $Eu_{0.5}Tb_{0.5}(H_2O)_5[W(CN)_8]$ compound (2.5 K) in comparison with the related $Eu(H_2O)_5[W(CN)_8]$ (2.8 K) suggests rather the random distribution of both lanthanides permitting the propagation of the ferromagnetic Tb-NC-W interactions through nonmagnetic Eu-NC-W-CN- linkages.

Finally, the mixed lanthanide compounds also present a partial light induced transition $W^{5+} \rightarrow W^{4+}$ which has not been observed for similar compounds containing only one lanthanide ion, i.e. $Eu(H_2O)_5[W(CN)_8]$ or $Tb(H_2O)_5[W(CN)_8]$ compounds. This photoluminescence reduction of tungsten has been evidenced by IR, EPR, and magnetism for $Eu_{0.5}Tb_{0.5}(H_2O)_5[W(CN)_8]$. As it has been suggested by theoretical calculations, the electronic rearrangement of Eu^{3+} and H_2O species in these networks is slightly different which apparently would favor the photoreduction of W^{5+} in $Eu_{0.5}Tb_{0.5}(H_2O)_5[W(CN)_8]$.

To conclude, the self-assembly of lanthanide ions with octacyanotungstate in two-dimensional coordination polymers networks seems to be a promising approach to achieve bifunctional magneto-luminescent molecule-based materials. Furthermore, the simultaneous use of two lanthanide ions in the same coordination polymer network offers additional advantages such as bifunctionality, multicolored emission, and ion−ion energy transfer.

4. EXPERIMENTAL SECTION

Syntheses. Unless otherwise noted, all manipulations were performed at ambient temperature using reagents and solvents as received. The precursor $(N(C_4H_9)_4)_3[W(CN)_8]\cdot 2H_2O$ was prepared as already described.[23] $[Ln(H_2O)_6](NO_3)_3$ (Ln = Eu^{3+}, Sm^{3+}) was purchased from ABCR, and $[Ln(H_2O)_6](NO_3)_3$ (Ln = Tb^{3+}, Gd^{3+}) was purchased from Rhodia. Acetonitrile and ether used in these experiments were analytical grade.

$Ln_{0.5}Ln'_{0.5}(H_2O)_n[W(CN)_8]$. The slow diffusion of a 0.10 M (6 mL) solution of $[(N(C_4H_9)_4]_3[W(CN)_8]\cdot 2H_2O$ and a mixture of two solutions 0.18 M (1.5 mL) of $[Ln(H_2O)_6](NO_3)_3$ (Ln = Eu^{3+}, Tb^{3+}) and 0.18 M (1.5 mL) of $[Ln'(H_2O)_6](NO_3)_3$ (Ln′ = Tb^{3+}, Gd^{3+}, Sm^{3+}) in acetonitrile leads to the formation of orange highly crystalline compounds after two weeks. The crystals were washed with acetonitrile and dried in air. The crystals are insoluble in the most common solvents and relatively stable in air. The composition of the crystalline compound was established by single-crystal X-ray diffraction at 160 K and by elemental analysis.

$Eu_{0.5}Tb_{0.5}(H_2O)_5[W(CN)_8]$, Orange Crystals. Elemental analysis: Calcd. for $C_8H_{10}N_8O_5Eu_{0.5}Tb_{0.5}W$, %: C, 15.06; Eu, 11.9; N, 17.57; Tb, 12.46; W, 28.84. Found: C, 15.78; Eu, 12.45; N, 17.88; Tb, 12.86; W, 29.34. IR (KBr): 2135 ; 2164 ; 2180 cm^{-1}.

$Eu_{0.5}Gd_{0.5}(H_2O)_5[W(CN)_8]$, Orange Crystals. Elemental analysis: Calcd. for $C_8H_{10}N_8O_5Eu_{0.5}Gd_{0.5}W$, %: C, 15.10; Eu, 11.95; Gd, 12.37; N, 17.62; W, 28.92. Found: C, 14.78; Eu, 12.68; Gd, 12.11; N, 18.28; W, 28.54. IR (KBr): 2132, 2163, 2179 cm^{-1}.

$Sm_{0.5}Tb_{0.5}(H_2O)_5[W(CN)_8]$, Orange Crystals. Elemental analysis: Calcd. for $C_8H_{10}N_8O_5Sm_{0.5}Tb_{0.5}W$, %: C, 15.10; N, 17.62; Sm, 11.83; Tb, 12.50; W, 28.92. Found: C, 15.98; N, 18.39; Sm, 11.37; Tb, 12.01; W, 29.47. IR (KBr): 2133, 2163, 2177 cm^{-1}.

Single-Crystal X-ray Diffraction. Single-crystals of $Ln_{0.5}Ln'_{0.5}(H_2O)_5[W(CN)_8]$ (where Ln/Ln′ = Eu^{3+}/Tb^{3+}, Eu^{3+}/Gd^{3+}, Sm^{3+}/Tb^{3+}) were manually harvested from the crystallization vials and mounted on either Hampton Research CryoLoops (using FOMBLIN Y perfluoropolyether vacuum oil (LVAC 140/13) purchased from Sigma-Aldrich),[24] with the help of a Stemi 2000 stereomicroscope equipped with Carl Zeiss lenses, or on glass fibers. Data for $Eu_{0.5}Tb_{0.5}(H_2O)_5[W(CN)_8]$ were collected at 150(2) K on a Bruker X8 Kappa APEX II charge-coupled device (CCD) area-detector diffractometer (Mo K_α graphite-monochromated radiation, λ = 0.71073 Å) controlled by the APEX2 software package[25] and equipped with an Oxford Cryosystems Series 700 cryostream monitored remotely using the software interface Cryopad.[26] Images were processed using the software package SAINT+,[27] and data were corrected for absorption by the multiscan semiempirical method implemented in SADABS.[28] Data for $Eu_{0.5}Gd_{0.5}(H_2O)_5[W(CN)_8]$ and $Sm_{0.5}Tb_{0.5}(H_2O)_5[W(CN)_8]$ were collected at 173(2) K on an Oxford Instruments Xcalibur Sapphire-2 charge-coupled device (CCD) area-detector diffractometer with a (Mo K_α graphite-monochromated radiation, λ = 0.71073 Å) controlled by the Crysalis^{Pro} software package.[29] Images were processed using the same general software package, and data were corrected for absorption (using spherical harmonics) by the multiscan semiempirical method implemented in SCALE3 ABSPACK of Crysalis^{Pro}.[30]

The crystal structures were solved employing the Patterson algorithm implemented in the software package SHELXS-97.[31] This approach allowed the immediate location of the metallic centers composing the two-dimensional networks. All remaining non-hydrogen atoms were directly located from difference Fourier maps calculated from successive full-matrix least-squares refinement cycles on F^2 using SHELXL-97.[31,32] All non-hydrogen atoms have been successfully refined using anisotropic displacement parameters.

The three collected data sets for this mixed-lanthanide system revealed that the bridging cyanide moieties, and most of the coordinated water molecules are affected by positional disorder, very much like that reported by us for the isotypical $Ln(H_2O)_5[M(CN)_8]$ system (where Ln = Sm^{3+}, Eu^{3+}, Gd^{3+}, or Tb^{3+} and M = Mo^{5+} or W^{5+}).[10] In the current structural models one coordinated water molecule [O(1W)] remains not affected by structural disorder. The second type of water molecule was, once again, found to be disordered over three distinct crystallographic positions, O(2W) and O(3W) (Figure 1a), with fixed rates of occupancy of 30%: 30%: 40% (calculated from an unrestrained model refinement). All cyanide ligands were equally disordered over two distinct crystallographic positions (Figure 1b). Even though the hydrogen atoms associated with the coordinated water molecules could not be located from difference Fourier maps, and attempts to include these in calculated positions did not lead to sensible structural refinements, they have been included in the empirical formulas of the materials (Table 1).

The last difference Fourier map synthesis showed the following: for $Eu_{0.5}Tb_{0.5}(H_2O)_5[W(CN)_8]$, the highest peak (1.816 eÅ^{-3}) and deepest hole (−4.536 eÅ^{-3}) located at 0.66 Å and 1.35 Å from O(1W); for $Eu_{0.5}Gd_{0.5}(H_2O)_5[W(CN)_8]$, the highest peak (0.501 eÅ^{-3}) and deepest hole (−1.758 eÅ^{-3}) located at 0.40 Å and 1.55 Å from N(2) and O(1W), respectively; for $Sm_{0.5}Tb_{0.5}(H_2O)_5[W(CN)_8]$, the highest peak (0.908 eÅ^{-3}) and deepest hole (−0.984 eÅ^{-3}) located at 0.67 Å and 0.49 Å from $Sm_{0.5}Tb_{0.5}$(1). Noteworthy, for $Eu_{0.5}Tb_{0.5}(H_2O)_5[W(CN)_8]$ the highest observed peak and hole are of high magnitude and usually close to the O(1W) water molecule (or to a metallic center). Attempts have been made to reduce these artifacts from the structural models by i) collecting different crystals, ii) using a slightly distinct absorption correction method, or even iii) reducing the resolution up to which the structure is reported, but the end models always showed the same limitations. In addition attempts were also made to model the O(1W) molecule as being disordered over two or more sites, but the refinements proved to be highly unstable which is a clear indication that this chemical entity is in fact not disordered.

Information concerning crystallographic data collection and structure refinement details is summarized in Table 1. Selected bond lengths (in Å) for the two crystallographically independent metallic coordination polyhedra present in the crystal structures are tabulated in Table 2. Structural drawings have been created using the software package Crystal Impact Diamond.[33]

Physical Measurements. Infrared spectra were recorded as KBr disks or Nujol mulls between NaCl plates on a Nicolet Model 510P spectrophotometer. Thermogravimetry (TG) analyses were performed using a Netzsch STA 409 instrument under argon atmosphere from 30 to 700 °C at a heating rate of 1 °C min^{-1}. Elemental analyses were performed by the Service Central d'Analyses (CNRS, Vernaison, France). The samples were heated at 3000 °C under He. Oxygen was

dx.doi.org/10.1021/ic301144j | Inorg. Chem. 2012, 51, 9005−9016

transformed in CO and detected by using an IR detector. Metals were determined with a high resolution ICP-MS using a ThermoFischer element. The photoluminescence spectra were recorded between 14 K and room temperature on a Fluorolog-3 Model FL3−2T with double excitation spectrometer and a single emission spectrometer (TRIAX 320) coupled to a R928 photomultiplier, using a front face acquisition mode. The excitation source was a 450 W xenon lamp. Emission was corrected for the spectral response of the monochromators, and the detector using a typical correction spectrum provided by the manufacturer and the excitation spectra were corrected for the spectral distribution of the lamp intensity using a photodiode reference detector. Magnetic susceptibility data were collected with a Quantum Design MPMS-XL SQUID magnetometer working in the temperature range 1.8−350 K and up to 7 T. The crystals have been grinded before placed in the sample holder. The magnetic measurements of all samples have been performed with the fast cooling of the samples to 10 K. Data were corrected for the sample holder and the diamagnetism contributions calculated from the Pascal's constants.[35] EPR measurements were performed on a Bruker Elexsys E 500 spectrometer (X-Band).

Computational Details. The VASP 4.6.3 computer code was used for all the density functional theory calculations.[34−36] These considered the PBE functional proposed by Perdew,[37] the projected augmented-wave (PAW) method as implemented in VASP[38,39] to take into account the effect of core electrons in the valence electron density, a cutoff of 450 eV for the plane waves expansion and a $3 \times 3 \times 3$ Monkhorst-Pack grid of special k-points[40] for the numerical integration in the reciprocal space. The convergence criteria were 10^{-6} eV for the total energy change and 10^{-3} eV/Å for the forces acting on the ions. The periodic calculations considered the experimental crystallographic unit cells; in all cases, the lattice vectors were kept fixed, and the atomic positions were fully relaxed. The optimization procedure was divided in two different stages. First, hydrogen atoms were added to O(1W), O(2W), and O(3W), and their positions were relaxed while the rest of atomic positions remained fixed. Then, in a second step, all the atomic positions were optimized.

■ ASSOCIATED CONTENT

Supporting Information

Additional luminescence and magnetic studies (SQUID magnetometry and EPR) and cif files. This material is available free of charge via the Internet at http://pubs.acs.org. Crystallographic data (including structure factors) for the structures reported in this paper have been deposited with the Cambridge Crystallographic Data Centre as supplementary publication nos. CCDC-753631 (for $Eu_{0.5}Tb_{0.5}(H_2O)_5[W(CN)_8]$), −753632 ($Eu_{0.5}Gd_{0.5}(H_2O)_5[W(CN)_8]$), and −753635 (for $Sm_{0.5}Tb_{0.5}(H_2O)_5[W(CN)_8]$). Copies of the data can be obtained free of charge on application to CCDC, 12 Union Road, Cambridge CB2 2EZ, U.K. FAX: (+44) 1223 336033. E-mail: deposit@ccdc.cam.ac.uk.

■ AUTHOR INFORMATION

Corresponding Author

*Fax: (33) 4 67 14 38 52, e-mail: joulia.larionova@univ-montp2.fr (J.L.). Fax: (351) 234 378 197, e-mail: lcarlos@ua.pt (L.D.C.).

Notes

The authors declare no competing financial interest.

■ ACKNOWLEDGMENTS

The authors thank Mme. Corine Rebeil (UM2, Institute Charles Gerhardt Montpellier, France) for magnetic measurements. The authors are grateful to *Fundação para a Ciência e a Tecnologia* (FCT, Portugal) for the financial support toward the purchase of the single-crystal diffractometer and funding (PPCDT/QUI/58377/2004 and PDTC/QUI-QUI/098098/2008). The authors also wish to thank CRUP-PAUILF (Portugal-France bilateral program), CNRS, the Université Montpellier II.

■ REFERENCES

(1) (a) *Functional Hybrids Materials*; Gomez-Romero, P., Sanchez, C., Eds.; Wiley-VCH Verlag GmbH&Co: KgaA Weinheim, Germany, 2004. (b) Torquato, S.; Hyun, S.; Donev, A. *Phys. Rev. Lett.* **2002**, *89*, 266601. (c) Torquato, S. Random *Heterogeneous Materials: Microstructure and Macroscopic Properties*; Springer-Verlag: New York, 2002. (d) Rabu, P.; Drillon, M. *Adv. Eng. Mater.* **2003**, *5*, 189. (e) Coe, B. J.; Curati, N. R. *Inorg. Chem. Commun.* **2004**, *25*, 147. (f) Knutson, J. I.; Martin, D. J.; Mitzi, D. B. *Inorg. Chem.* **2005**, *44*, 4699. (g) Gruselle, M.; Train, C.; Boubekeur, K.; Gredin, P.; Ovanesyan, N. *Coord. Chem. Rev.* **2006**, *250*, 2491.

(2) (a) Rikken, G. L.; Raupach, E. *Nature* **2000**, *405*, 932. (b) Minguet, M.; Luneau, D.; Lhotel, E.; Villar, V.; Paulsen, C.; Amabilino, D. B.; Veciana, J. *Angew. Chem., Int. Ed.* **2002**, *41*, 586. (c) Kumagai, H.; Inoue, K. *Angew. Chem., Int. Ed.* **1999**, *38*, 1601. (d) Barron, L. D. *Nature* **2000**, *504*, 895. (e) Yamaguchi, I.; Fujinaga, E.; Ozeki, T.; Yamamoto, T. *Bull. Chem. Soc. Jpn.* **2004**, *77*, 1773.

(3) (a) Bénard, S.; Pei, Y.; Audiére, J.-P.; Rivière, E.; Clément, R.; Ghilhem, J.; Tchertanov, L.; Nakatani, K. *J. Am. Chem. Soc.* **2000**, *122*, 9444. (b) Bénard, S.; Léaustic, A.; Pei, Y.; Clément, R. *Chem. Mater.* **2001**, *13*, 159. (c) Liu, C.-M.; Zuo, J.-L.; Zhang, D.-Q.; Zhu, D.-B. *CrystEngComm* **2008**, 1674. (d) Masciocchi, N.; Galli, S.; Sironi, A.; Cariati, E.; Galindo, M. A.; Barea, E.; Romeno, A.; Salas, J. M.; Navarro, J. A. R.; Santoyo-Gonzalez, F. *Inorg. Chem.* **2006**, *45*, 7612.

(4) (a) Coronado, E.; Galàn-Mascaros, J.-R.; Gomez-Garcia, C. J.; Laukhin, V. *Nature* **2000**, *408*, 447. (b) Setifi, F.; Ouahab, L.; Golhen, S.; Yoshida, Y.; Saito, G. *Inorg. Chem.* **2003**, *42*, 1791. (c) Maspoch, D.; Ruiz-Molina, D.; Veciana, J. *Chem. Soc. Rev.* **2007**, *36*, 770. (d) Patil, R. M.; Shivkumar, R. *Asian J. Chem.* **2008**, *20*, 4477.

(5) Harbuzaru, B. V.; Corma, A.; Rey, F.; Atienzar, P.; Jorda, J. L.; Garcia, H.; Ananias, D.; Carlos, L. D.; Rovha, J. *Angew. Chem., Int. Ed.* **2008**, *47*, 1080.

(6) (a) Niel, V.; Thompson, A. L.; Munoz, M. C.; Galet, A.; Goeta, A. S. E.; Real, J. A. *Angew. Chem., Int. Ed.* **2003**, *42*, 3760. (b) Bonhommeau, S.; Molnar, G.; Galet, A.; Zwick, A.; Real, J. A.; McGarvey, J. J.; Bousseksou, A. *Angew. Chem., Int. Ed.* **2005**, *44*, 4069. (c) Lange, C. W.; Foldeaki, M.; Nevodchikov, V. I.; Cherkasov, V. K.; Abakumov, G. A.; Pierpont, C. G. *J. Am. Chem. Soc.* **1992**, *114*, 4220. (d) Hendrickson, D. N.; Pierpont, C. G. In *Spin Crossover in Transition Metal Compounds II, Top. Curr. Chem.*; Gütlich; P., Goodwin, H. A., Eds.; Springer-Verlag: Heidelberg, 2004; Vol. *233*, p 63.

(7) (a) Maspoch, D.; Domingo, N.; Ruiz-Molina, D.; Wurst, K.; Vaughan, G.; Tejada, J.; Rovira, C.; Veciana, J. *Angew. Chem., Int. Ed.* **2004**, *43*, 1828. (b) Maspoch, D.; Domingo, N.; Ruiz-Molina, D.; Wurst, K.; Tejada, J.; Rovira, C.; Veciana, J. *J. Am. Chem. Soc.* **2004**, *126*, 730. (c) Luo, F.; Che, Y.; Zheng, J. *Cryst. Growth Des.* **2009**, *9*, 1066. (d) Maspoch, D.; Molina, D. R.; Veciana, J. *Chem. Soc. Rev.* **2007**, *36*, 770. (e) Kaneko, W.; Ohba, M.; Kitagawa, S. *J. Am. Chem. Soc.* **2007**, *129*, 13706. (f) Yanai, N.; Kaneko, W.; Yoneda, K.; Ohba, M.; Kitagawa, S. *J. Am. Chem. Soc.* **2007**, *129*, 3496. (g) Kurmoo, M.; Kumagai, H.; Chapman, K. W.; Kepert, C. J. *Chem. Commun.* **2005**, 3012.

(8) (a) Aumuller, A.; Erk, P.; Klebe, G.; Hünig, S.; von Schütz, J. U.; Werner, H. P. *Angew. Chem., Int. Ed. Engl.* **1986**, *25*, 740. (b) Kitagawa, H.; Nagao, Y.; Fujishima, M.; Ikeda, R.; Kanda, S. *Inorg. Chem. Commun.* **2003**, *6*, 346.

(9) (a) Rueff, J.-M.; Nierengarten, J.-F.; Gilliot, P.; Demessence, A.; Gregut, O.; Drillon, M.; Rabu, P. *Chem. Mater.* **2004**, *16*, 2933. (b) Kahn, O.; Cador, O.; Larionova, J.; Mathonier, C.; Sutter, J.-P. *Mol. Cryst. Liq. Cryst.* **1997**, *305*, 1. (c) Decurtins, S.; Schmalle, H.; Pellaux, R.; Schneuwly, Ph.; Hauser, A. *Inorg. Chem.* **1996**, *35*, 1451.

(10) (a) Chelebaeva, E.; Larionova, J.; Guari, Y.; Ferreira, R. A. S.; Carlos, L. D.; Paz, F. A. A.; Trifonov, A.; Guerin, Ch. *Inorg. Chem.* **2008**, *47*, 775. (b) Chelebaeva, E.; Larionova, J.; Guari, Y.; Ferreira, R. A. S.; Carlos, L. D.; Almeida Paz, F. A.; Trifonov, A.; Guérin, Ch. *Inorg. Chem.* **2009**, *48*, 5983. (c) Long, J.; Chelebaeva, E.; Larionova, J.; Guari, Y.; Ferreira, R. A. S.; Carlos, L. D.; Almeida Paz, F. A.; Trifonov, A.; Guérin, C. *Inorg. Chem.* **2011**, *50*, 9924.

(11) Benelli, C.; Gatteschi, D. *Chem. Rev.* **2002**, *102*, 2369.

(12) (a) Bunzli, J.-C. *Acc. Chem. Res.* **2006**, *39*, 53. (b) Cotton, S. *Lanthanide and actinide chemistry*; Wiley: 2006.
(13) (a) Evans, R. C.; Carlos, L. D.; Douglas, P.; Rocha, J. *J. Mater. Chem.* **2008**, *18*, 1100. (b) Biju, S.; Ambili Raj, D. B.; Reddy, C. K.; Cowley, A. H.; Findlater, M. *J. Mater. Chem.* **2009**, *19*, 1425. (c) Podhoroecki, A.; Banski, M.; Misiewicz, J.; Afzaal, M.; O'Brien, P.; Cha, D.; Wang, X. *J. Mater. Chem.* **2012**, *22*, 5356.
(14) (a) Larionova, J.; Willemin, S.; Donnadieu, B.; Henner, B.; Guérin, C.; Gillon, B.; Goujon, A. *J. Phys. Chem. Solids* **2004**, *65*, 677. (b) Rombaut, G.; Verelst, M.; Golhen, S.; Ouahab, L.; Mathoniere, C.; Kahn, O. *Inorg. Chem.* **2001**, *40*, 1151. (c) Rombaut, G.; Mathoniere, C.; Guionneau, P.; Golhen, S.; Ouahab, L.; Verelst, M.; Lecante, P. *Inorg. Chim. Acta* **2001**, *326*, 27. (d) Rombaut, G.; Golhen, S.; Ouahab, L.; Mathoniere, C.; Kahn, O. *J. Chem. Soc., Dalton Trans.* **2000**, 3609. (e) Sra, A. K.; Andruh, M.; Kahn, O.; Golhen, S.; Ouahab, L.; Yakhmi, J. V. *Angew. Chem., Int. Ed.* **1999**, *38*, 2606. (f) Lu, J.; Harrison, W. T. A.; Jacobson, A. J. *Angew. Chem., Int. Ed. Engl.* **1995**, *34*, 2557.
(15) Bleuzen, A.; Marvaud, V.; Mathonière, C.; Sieklucka, B.; Verdaguer, M. *Inorg. Chem.* **2009**, *48*, 3453 and references therein.
(16) Benelli, C.; Caneschi, A.; Gatteschi, D.; Pardi, L.; Rey, P. *Inorg. Chem.* **1989**, *28*, 275.
(17) Carlin, R. L. *Magnetochemistry*; Springer: Berlin, 1997.
(18) (a) Evangelisti, M.; Kahn, M. L.; Bartolomé, J.; de Jongh, L. J.; Meyers, C.; Leandri, J.; Leroyer, Y.; Mathoniere, C. *Phys. Rev. B* **2003**, *68*, 2534. (b) Orton, J. W. *EPR. An Introduction to Transition Group Ions in Crystals*; Gordon and Breach: New York, 1968. (c) Sen, H.; Neogy, D.; Wanklyn, B. M. *J. Magn. Magn. Mater.* **1988**, *73*, 221.
(19) Mydosh, J. A. *Spin Glasses*; Taylor and Francis: WA, 1993.
(20) Seiklucka, B. *Inorg. Chim. Acta* **1991**, *186*, 179.
(21) Malta, O. L. *J. Non-Cryst. Solids* **2008**, *354*, 4770.
(22) Rocha, J.; Carlos, L. D.; Almeida Paz, F. A.; Ananias, D. *Chem. Soc. Rev.* **2011**, *40*, 926.
(23) Corden, B. J.; Cunningham, J. A.; Eisenberg, R. *Inorg. Chem.* **1970**, *9*, 356.
(24) Kottke, T.; Stalke, D. *J. Appl. Crystallogr.* **1993**, *26*, 615.
(25) APEX2, *Data Collection Software Version 2.1-RC13*; Bruker AXS: Delft, The Netherlands, 2006.
(26) Cryopad, *Remote monitoring and control, Version 1.451*; Oxford Cryosystems: Oxford, United Kingdom, 2006.
(27) SAINT+, *Data Integration Engine v. 7.23a*, 1997−2005; Bruker AXS: Madison, Wisconsin, USA.
(28) Sheldrick, G. M. *SADABS v.2.01, Bruker/Siemens Area Detector Absorption Correction Program*; Bruker AXS: Madison, Wisconsin, USA, 1998.
(29) *CrysalisPro Software Package, Version 1.171.34.40, Xcalibur Single Crystal CCD Diffractometer*; Agilent Technologies: Yarnton, England, 2010.
(30) *SCALE3 ABSPACK: Empirical absorption correction: CrysAlis - Software Package*; Oxford Diffraction Ltd.: 2006.
(31) (a) Sheldrick, G. M. *SHELXS-97, Program for Crystal Structure Solution*; University of Göttingen: 1997. (b) Sheldrick, G. M. *Acta Crystallogr., Sect. A: Found. Crystallogr.* **2008**, *64*, 112−122.
(32) Sheldrick, G. M. *SHELXL-97, Program for Crystal Structure Refinement*; University of Göttingen: 1997.
(33) Brandenburg, K. *DIAMOND, Version 3.2f*; Crystal Impact GbR: Bonn, Germany, 1997−2010.
(34) Kresse, G.; Hafner, J. *Phys. Rev. B* **1993**, *47*, 558.
(35) Kresse, G.; Furthmüller. *J. Comput. Mater. Sci.* **1996**, *6*, 15.
(36) Kresse, G.; Furthmüller, J. *Phys. Rev. B* **1996**, *54*, 11169.
(37) Perdew, J. P.; Burke, K.; Ernzerhof, M.
(38) Blöchl, P. E. *Phys. Rev. B* **1994**, *50*, 17953.
(39) Kresse, G.; Joubert, D. *Phys. Rev. B.* **1999**, *59*, 1758.
(40) Monkhorst, H. J.; Pack, J. D. *Phys. Rev. B.* **1976**, *13*, 5188.